Hydrothermal Aging of Polyimide Film

*Christina Anna Braun, Seo Lin Nam, A. Paulina de la Mata, James J. Harynuk, Hyun-Joong Chung, Patricia Isabelle Dolez**

Dr. Christina Anna Braun, Dr. Seo Lin Nam, Dr. A. Paulina de la Mata, Prof. James J. Harynuk, Prof. Hyun-Joong Chung, Prof. Patricia I. Dolez

Department of Human Ecology, University of Alberta, Edmonton, Alberta T6G 2N1, Canada
Department of Chemical and Materials Engineering, University of Alberta, Edmonton, Alberta T6G1H9, Canada
Department of Chemistry, University of Alberta, Edmonton, Alberta T6G 2G2, Canada
E-mail: pdolez@ualberta.ca

Keywords: polyimide, hydrothermal aging, hydrolysis, tensile strength, chemical analysis, chemometrics, end-of-life sensor

Abstract: The hydrothermal aging of a commercial polyimide film, (poly(pyromellitic dianhydride-co-4,4'-oxydianiline)) is investigated, providing further insight into the well-known loss of properties that can occur for these materials in the presence of moisture. The study involved measuring ATR-FTIR, ultimate tensile strength, and percent elongation at break, under accelerated hydrothermal aging conditions at three different temperatures (70, 80, and 90 °C). ATR-FTIR data was analyzed using chemometrics in order to identify significant trends that develop upon the accelerated aging conditions. The most dramatic changes were observed for the aging at 90 °C. Changes in the ATR-FTIR spectra for aging at all three temperatures can be attributed to hydrolysis of the imide groups. Ultimate tensile strength was also used to monitor the hydrothermal aging process. This data was used to construct an Arrhenius plot from which an activation energy of 71.8 KJ/mol was determined for the hydrothermal aging process. This value is comparable to that of textiles used in fire protective clothing, suggesting that polyimide is a viable candidate for modeling the degradation of these textiles. This paper also shows the large potential of chemometrics for polymer aging studies as it allows identifying degradation mechanisms from subtle chemical changes in the materials.

1. INTRODUCTION

Polyimides are an incredibly useful family of high-performance polymers that combines mechanical toughness, chemical and thermal resistance, a low dielectric constant, and a low thermal expansion coefficient.[1] In particular, aromatic polyimides are known for their ability to operate within a very wide temperature range, with the most well-known polyimide, Kapton® developed by DuPont, having been successfully employed in applications with temperatures as low as –269 °C and as high as 400 °C.[1b] This remarkable thermal stability, in addition to many other desirable properties, has led to the use of polyimides in a very broad range of fields including electronics, aerospace, and the military.[1a,2] More specifically, polyimides are frequently used as insulating coatings for wires/electronics as well as high temperature structural adhesives. Other applications for polyimides that have been studied extensively include reinforced nanocomposites[3] and gas separation membranes.[4] Furthermore, there is a significant interest in the use of polyimides in optoelectronic display technologies; however, low processability (due to a lack of solubility) as well as poor optical transparency are challenges that must first be overcome.[5]

The remarkable thermal stability of polyimides is attributed to a very rigid, aromatic structure.[1,2] One popular method for the formation of aromatic polyimides includes reacting aromatic diamines (or diisocyanates) with aromatic dianhydrides, which initially forms a poly(amic acid) intermediate. The poly(amic acid) can be converted into a polyimide through prolonged heating which results in the formation of imide rings accompanied by the elimination of water. Generally, the combination of electron-rich diamines with electron-poor dianhydrides results in deeply colored polyimides due to the formation of intra- and intermolecular charge transfer interactions. Figure 1 shows the structure of poly(pyromellitic dianhydride-co-4,4'-oxydianiline), which forms deep orange films, and was used in this study. FTIR can be used to monitor the thermal curing, with imidization being indicated by the

disappearance of amide/carboxylic acid peaks and the emergence of imide peaks.[6a] For the polyimide shown in Figure 1, there are four peaks corresponding to the imide functional groups, which occur at 1778, 1378, 721, and 588 cm^{-1}.[6]

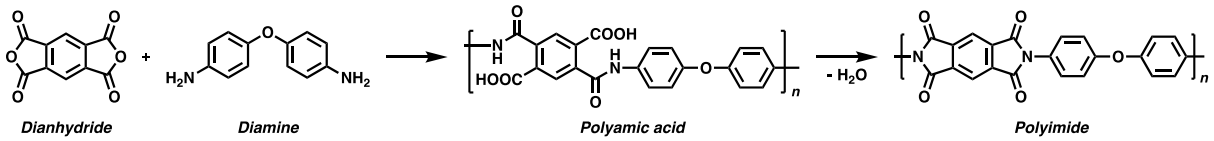

Figure 1. The synthesis of the polyimide used in this study from aromatic dianhydrides and aromatic diamines.

Despite their impressive chemical and thermal stability, several studies have demonstrated negative effects of moisture diffusion/sorption on the properties of polyimide films. For example, Kapton® film can absorb up to 3 wt% of water from atmospheric humidity;[7a] the absorbed water has been linked to an increase in dielectric permittivity and decrease in electrical resistivity, and can also lead to mechanical failures (cracks, delamination, loss of adhesion, etc.).[7] In fact, a linear correlation has been found between the relative dielectric constant at a given temperature and the amount of absorbed water, leading to the early use of polyimides as a relative humidity sensor.[8] Furthermore, moisture-based degradation at elevated temperatures results in a substantial deterioration of the mechanical strength of polyimide films.[9] Plasticization by water at high temperature has also been observed, leading to a reduction in the material's mechanical performance when tested in the wet state.[9c] However, despite the well-known negative effects that moisture can pose to polyimides, the origin behind these observed degradations is not well understood. Because of the importance of polyimides in such a broad range of applications, developing a better understanding behind the mechanism of hydrothermal aging of polyimide is essential.

The moisture-based degradation of polymers is typically attributed to chain scission via hydrolysis, particularly in the case of polymers formed via condensation reactions.[10] In 1971, DeIasi was one of the first researchers to study the aqueous degradation of polyimides by immersing samples in water at temperatures of up to 100 °C and monitoring the decrease in ultimate tensile strength of the aged samples.[9a] He proposed that the diminished strength was due to hydrolysis of amide or carboxylic acid groups which are often present in small quantities, rather than hydrolysis of the imide rings which are typically stable towards hydrolysis under neutral conditions. In a more recent study, the hydrothermal aging of another polyimide (HFPE-II-52) was studied using a sealed tube maintaining an environment of 100% RH at elevated temperatures.[9b] The authors studied the aged samples by measuring compression strength, and concluded that hydrolysis of the imide groups is rampant at temperatures ≥ 250 °C, but is not significant below 200 °C. Although these studies provide valuable information on the effect of hydrothermal aging on polyimides at extreme temperatures, the effect of hydrothermal aging under less extreme conditions is still unclear. Furthermore, the extent/role of hydrolysis of the imide groups when polyimide is exposed to high levels of moisture remains unclear.

Despite the abovementioned methods for characterizing aged specimens (including mechanical analysis), a simple, quick and non-destructive technique would be highly beneficial for further studying aged samples. Although FTIR is a valuable and non-destructive technique, it is very difficult to monitor small changes and draw precise conclusions. In this regard, chemometrics has emerged as a powerful data analysis methodology which uses mathematical and statistical methods to extract meaningful information out of very large datasets.[11] Among various chemometric techniques, principal component analysis (PCA) is a dimensionality-reduction method that computes new sets of uncorrelated variables (called principal components) and has been commonly used for the exploration of large data sets.[11]

As a specific example, there is increasing interest in ATR-FTIR spectroscopy combined with chemometrics analysis, where chemometrics is used as a sensitive and objective tool to differentiate between different groups in the study.[12] One hallmark of combining ATR-FTIR with chemometrics is that it enables the opportunity to explore full and complete data sets, which often results in the discovery of subtle, objective trends while minimizing outside influence.

A better characterization and understanding of the hydrothermal aging of polyimide is also needed for a new potential application of targeting protective clothing against heat and flame. One important use of heat-resistant polymers is the development of fibers for fire protective clothing.[13] These fibres are typically made from high performance synthetic polymers; some common examples include polyaramids (*e.g.* Kevlar®, Nomex®), polybenzoxazoles (*e.g.* Zylon®), and polybenzimidazole (PBI). Although these materials (and the resulting fibres) are stable at high temperatures, they are known to degrade slowly upon exposure to excessive heat, UV-light, and moisture, which can all result in the deterioration of performance before any signs of degradation are visible.[14] To overcome this problem, Dolez, Chung and coworkers have proposed the concept of an end-of-life sensor for fire protective clothing which involves a thin "sensing" polymeric layer that slowly deteriorates over time when exposed to the conditions the high-performance fibers are sensitive to.[15] To this end, polyimides may be an ideal candidate for an end-of-life sensor for the moisture-based degradation of fire protective clothing.

In this paper, we study the moisture-based degradation of a commercial polyimide film under accelerated hydrothermal aging conditions. The residual ultimate tensile strength (UTS) of the hydrothermally aged samples was measured for different exposure times and temperatures. An Arrhenius plot was constructed from the UTS data by application of the time-temperature

superposition principle. The activation energy obtained for the moisture-based degradation of the polyimide film was compared to values of the activation energy reported for the moisture-based degradation of fabrics used in fire protective clothing. Finally, the aged polyimide specimens were studied via FTIR and analyzed using chemometrics to elucidate the mechanisms involved in the hydrothermal degradation of the polyimide film between 70 and 90 °C.

2. EXPERIMENTAL AND METHODOLOGIES

2.1. Materials

The material used in this study was a thermoplastic (as defined by the manufacturer) polyimide film (XF-137, thickness of 125 μm) purchased from Polyonics (New Hampshire, USA).

2.2. Accelerated Hydrothermal Aging

Accelerated aging was performed to investigate the effect of hydrothermal aging on the mechanical integrity and chemical composition of the polyimide film. For this study, 150 mm x 10 mm specimens were fully immersed in reverse-osmosis (RO) water, by hanging them inside a jar from a stainless steel mesh disk (Figure 2), and stored in an oven at temperatures of 70, 80, and 90 °C for up to 1344h (56 days). Aged samples were periodically collected and studied. RO water heated at the set oven temperature was added at regular intervals in the jars to compensate for evaporation.

Figure 2. Picture of the water aging setup.

2.3. Mechanical Tests

The effect of the accelerated hydrothermal aging was monitored using UTS measurements. Tensile strength was measured on the aged specimens using an Instron 5943 (Massachusetts, USA) mechanical test frame equipped with a 1kN load cell. The test was conducted at a deformation rate of 50 mm min^{-1} with a gauge length of 100 mm according to ASTM D882. The UTS was computed by dividing the force required to break the specimen by its original cross-sectional area. At least five specimens were tested for each condition. The percent elongation at break was calculated by taking the ratio of the original length (100 mm) by the final length at the breaking point.

2.4. Calculation of the Activation Energy

The Arrhenius model has been used extensively to predict the activation energy and/or lifetime of a material under specific aging conditions.[16] This model operates under two main assumptions. The first assumption is that the degradation is homogeneous and caused by a single chemical reaction following the kinetic relationship:

$$\frac{dC}{dt} = KC^{\alpha}$$

where C is the concentration of a chemical species, K is the rate constant of the reaction, and α is the reaction order. Secondly, the Arrhenius model assumes that K varies with temperature according to the following equation:

$$\boldsymbol{K = K_0 \exp\left(-\frac{E_a}{RT}\right)}$$

Where E_a is the activation energy for the reaction, R is the universal gas constant, and T is the absolute temperature. This latter assumption implies that by collecting data under accelerating aging conditions (*e.g.* elevated temperatures) we can extrapolate data to make predictions about the activation energy (or lifetime) of a process that occurs over much longer time periods and are thus difficult to measure.

In combination with the Arrhenius model, the time-temperature superposition (TTS) principle was used to analyze the data.[17] This principle applies to linear, viscoelastic materials and assumes that property-loss versus time plots have identical shapes for different aging temperatures when expressed as a function of the logarithm of time. Therefore, by determining a constant shift factor for each temperature, data collected at different temperatures can be translated such that the entire data set forms one smooth curve.

To construct the Arrhenius plot, the residual UTS data for specimens aged at 70, 80 and 90 °C were plotted as a function of the hydrothermal aging time on a semi-logarithmic scale. Next, the time-temperature superposition (TTS) approach was used in order to construct a master curve using shift factors. The temperature of 70 °C was used as a reference. Shift factors translating the data collected at 80 and 90 °C were empirically determined in order to obtain a smooth curve that covers the entire data set. Finally, the Arrhenius plot was constructed by expressing the natural logarithmic of the shift factors as a function of the inverse absolute temperature, allowing the activation energy to be calculated from the slope of this plot.

2.5. ATR-FTIR Analyses

All ATR-FTIR spectra were recorded in absorption mode using a Nicolet™ Continuum™ FTIR Microscope (Thermo Scientific, Canada). The main bench is a Nicolet 8700 equipped with a narrow-band mercury cadmium telluride (MCT) detector, and a micro-ATR accessory with a Ge tip (Thermo Scientific, Canada) was used. For the measurement, the specimen was placed on a support and then the Ge crystal tip was lowered to contact the sample. Spectra were recorded in the range from 4000 cm^{-1} to 650 cm^{-1} with a resolution of 4 cm^{-1}. For each acquisition (background and sample) 128 scans were averaged. For each condition (aging temperature and duration), six different polymer samples were used as the condition replicates for the analysis. FTIR analyses were conducted within the mechanical testing area (omitting 2.5 cm on each end which are required for the grip) before mechanical tests were conducted (aging and measurement schedule in Supporting Information, Table S1-3). A total of three ATR-FTIR measurements were taken within the center 10 cm for each specimen, as marked with an "X" in Figure 3. For control samples, unaged polymer strips were measured using the identical conditions as for the aged samples and the same data were used for the chemometric analysis for all three different hydrothermal aging temperatures. Furthermore, one unaged polymer specimen was chosen as the quality control (QC) and was measured prior to measuring all of the aged samples in order to account for day-to-day variations.

Figure 3. Illustrative representation of a polymer strip, with ATR-FTIR measurement sites indicated by an "X".

2.6. Chemometric Analysis

The chemometric analyses were performed in MATLAB R2017a, Windows 64-bit version (The Mathworks Inc., Natick, MA, USA), using PLS Toolbox (R8.5.2; Eigenvector Research Inc., Wenatchee, WA, USA). Each dataset of the ATR-FTIR spectra at the respective hydrothermally aged temperature was preprocessed according to published guidelines,[18] including a baseline correction (Automatic weighted least squares, dim = 2, order = 2), followed by multiplicative scatter correction (MSC, mean) and was mean-centred prior to the principal component analysis (PCA). PCA was applied with cross-validation to explore the general clustering of the data.

3. RESULTS

3.1. Ultimate Tensile Strength and Percent Elongation at Break

Before subjecting the polyimide to the aging conditions, the UTS of the commercial film as received was measured to be 150 ± 3 MPa. The results for the UTS and percent elongation at break after accelerated hydrothermal aging at 70, 80, and 90 °C are shown in Figures 4 and 5, respectively. A clear decrease in the UTS and elongation at break is observed for all three aging temperatures. This decrease occurs faster at higher aging temperatures; after 4 weeks of hydrothermal aging at 90 °C, the UTS decreased to 64 ± 2 MPa, which represents a value that is 43% of the original UTS for unaged polyimide film.

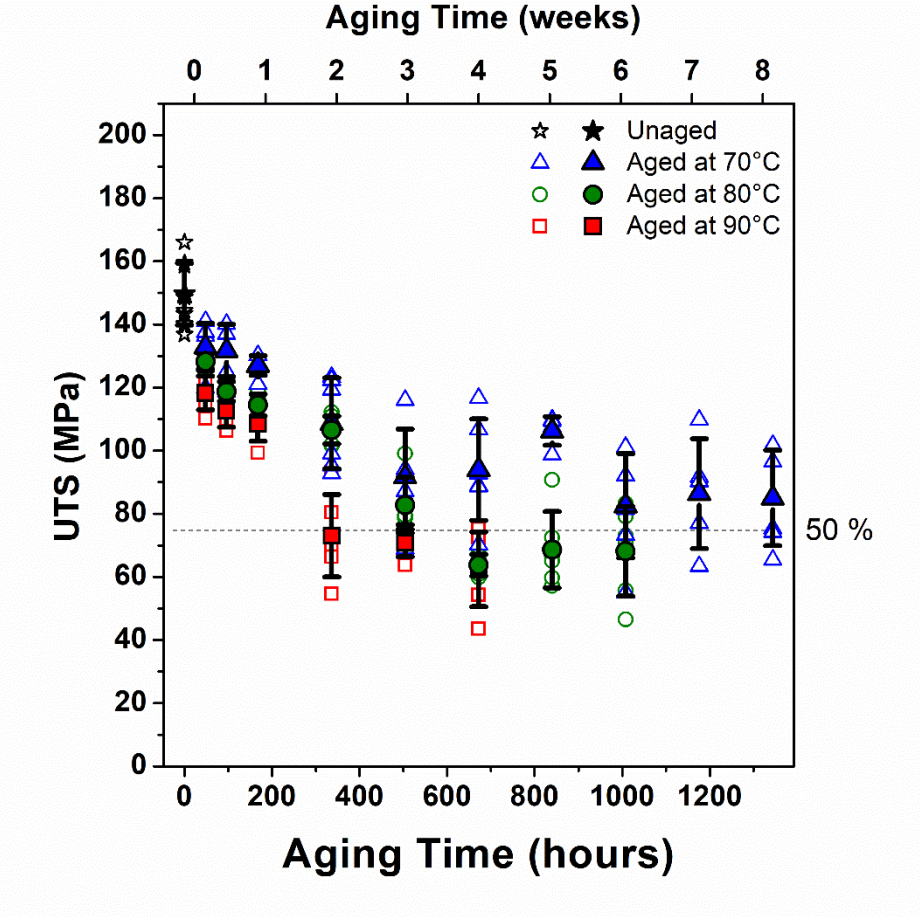

Figure 4. Ultimate tensile strengths (UTS) of unaged polyimide film (black stars), as well as polyimide films that have been hydrothermally aged at 70 °C (blue triangles), 80 °C (green circles) and 90 °C (red squares) as a function of the aging time. The average values are identified with solid symbols and the results for the individual specimens by open symbols. A horizontal dashed line represents 50 % of the ultimate tensile strength for the unaged polyimide.

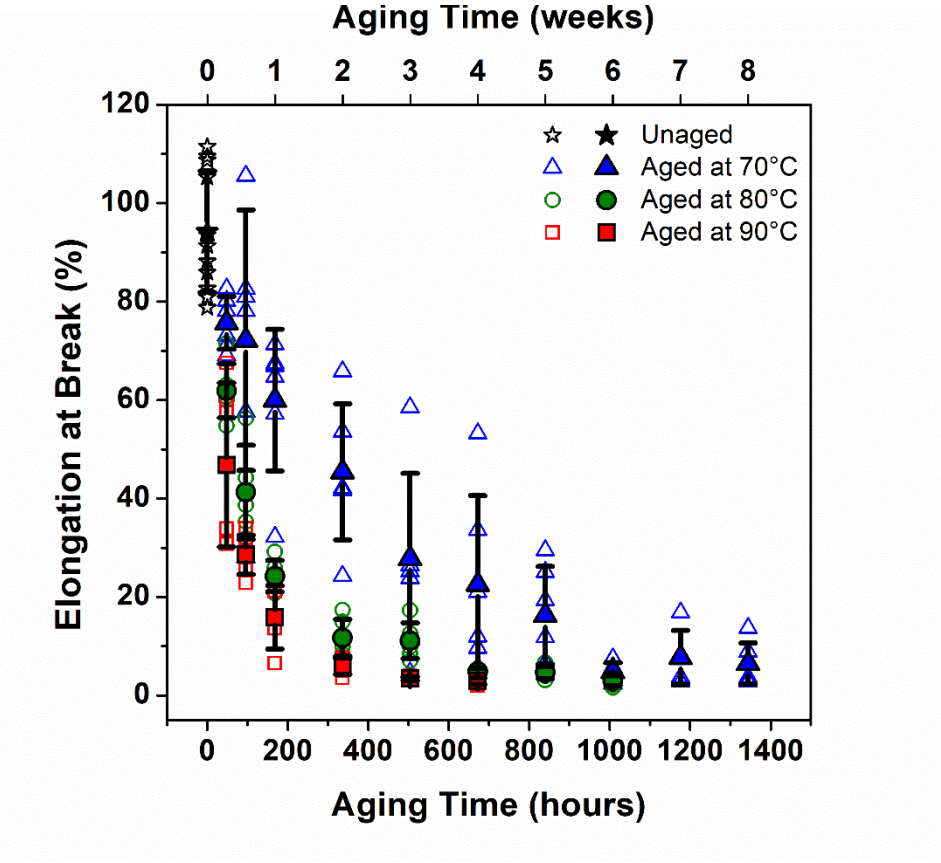

Figure 5. Percent elongation of unaged polyimide film (black stars), as well as polyimide films that have been hydrothermally aged at 70 °C (blue triangles), 80 °C (green circles) and 90 °C (red squares) as a function of the aging time. The average values are identified with solid symbols and the results for the individual specimens by open symbols.

3.2. Calculation of the Activation Energy for Hydrothermal Aging

The activation energy was calculated from an Arrhenius plot constructed using the UTS data of hydrothermally aged polyimide samples. The master curve is shown in Figure 6 and the shift factors are presented in Table 1. The shift factors were used to construct the Arrhenius plot shown in Figure 7, which could be fitted with a straight line. From the slope of the Arrhenius plot, the activation energy for the hydrothermal aging of polyimide was calculated to be 71.8 ± 0.1 kJ/mol. This result is comparable to the value of 63 kJ/mol reported by DeIasi and Russel for the effect of hydrothermal aging in DI water between 25 and 100°C on the tensile strength of polyimide.[9a]

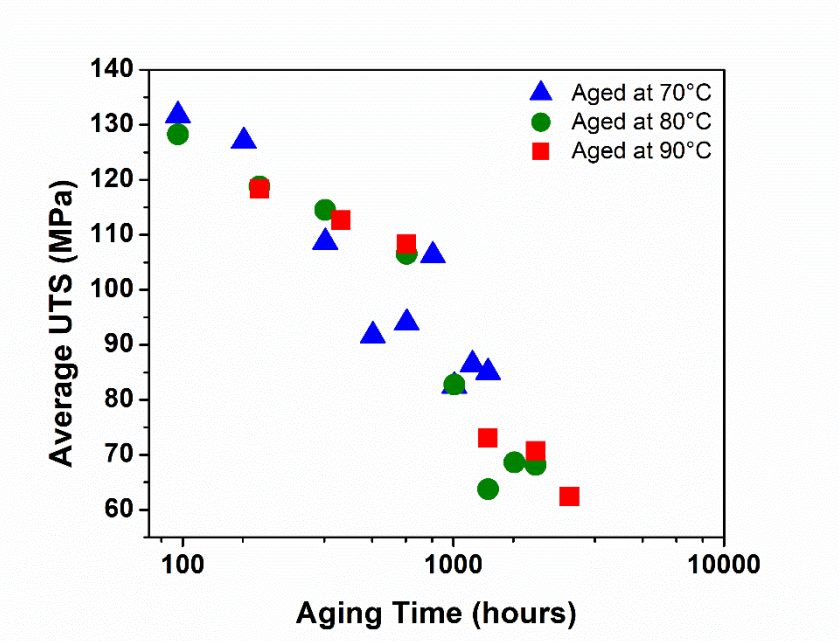

Figure 6. Time temperature superposition (TTS) master curve for the hydrothermal aging of polyimide at 70 °C (blue triangles), 80 °C (green circles) and 90 °C (red squares).

Table 1. Empirical shift factors used in the time temperature superposition master curve.

Aging Temperature (°C)	Empirical Shift Factor
70	1
80	2
90	4

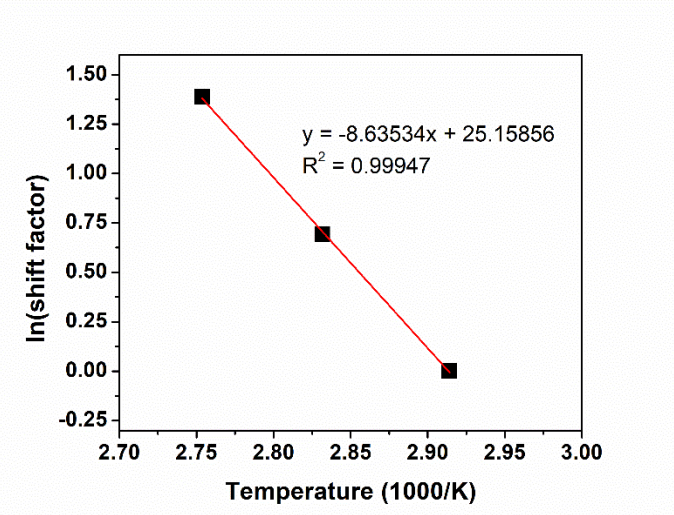

Figure 7. Arrhenius for the hydrothermal aging of the polyimide film.

3.3. FTIR Analysis

As mentioned previously, the FTIR spectrum of polyimide has four bands corresponding to the imide functional group, and these occur at 1776, 1716, 1373, and 722 cm^{-1} for the polyimide used in this study. Figure 8 shows the FTIR spectrum for the unaged commercial film that was used in this study (a), as well as examples of spectra for the hydrothermally aged samples (b-d). The band assignments for unaged polyimide are listed in **Table S**4 in Supporting Information.

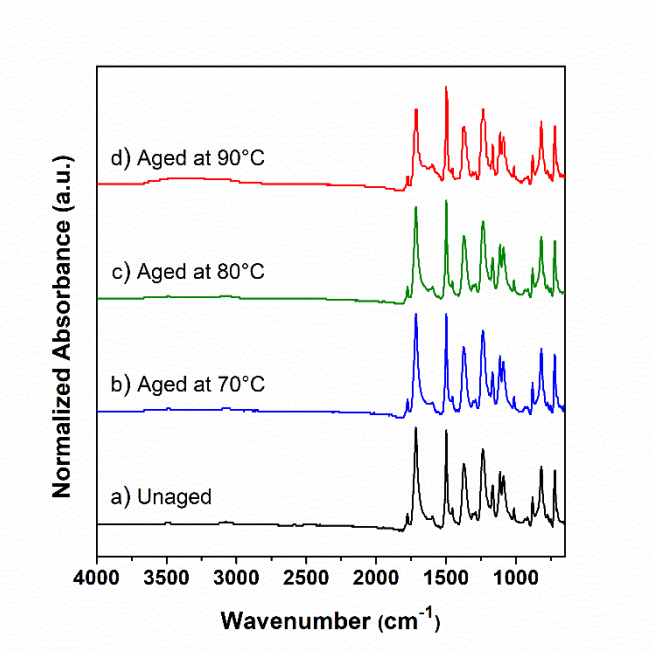

Figure 8. Stacked FTIR spectra of a) unaged polyimide film (black), b) polyimide film hydrothermally aged for 8 weeks at 70 °C (blue), c) polyimide film hydrothermally aged for 6 weeks at 80 °C (green), and d) polyimide film hydrothermally aged for 4 weeks at 90 °C (red). Each spectrum is plotted as normalized absorbance.

3.4. Chemometric Analysis of FTIR Data

The dataset at each of the different aging temperatures was comprised of a control (non-aged PI film), a quality control (a selected non-aged specimen, remeasured), and hydrothermally aged samples for various durations of time. The dataset of 70 °C, 80 °C, and 90 °C contained a total of 189, 138, and 99 spectra, respectively, with 1738 variables from 650 cm^{-1} to 4000 cm^{-1}. For each dataset, a PCA model was constructed for exploratory analysis and the top two principal components (PCs) representing the largest variance (PC1) and second-largest variance (PC2) described in the data were selected for the construction of score plots. Two-dimensional score plots using the first two principal components are shown in Figure 9, with scores on PC1 corresponding to the horizontal-axis while scores on PC2 correspond to the

vertical axis. In both cases, the percentage that the score accounts for based on the total variance is indicated in parenthesis on the axis label. Four outliers were removed based on Hotelling T^2 and Q residual values[19] (see Supporting Information, Figure S1) for both the datasets of 70 °C and 80 °C, resulting in 185 and 134 samples, respectively.

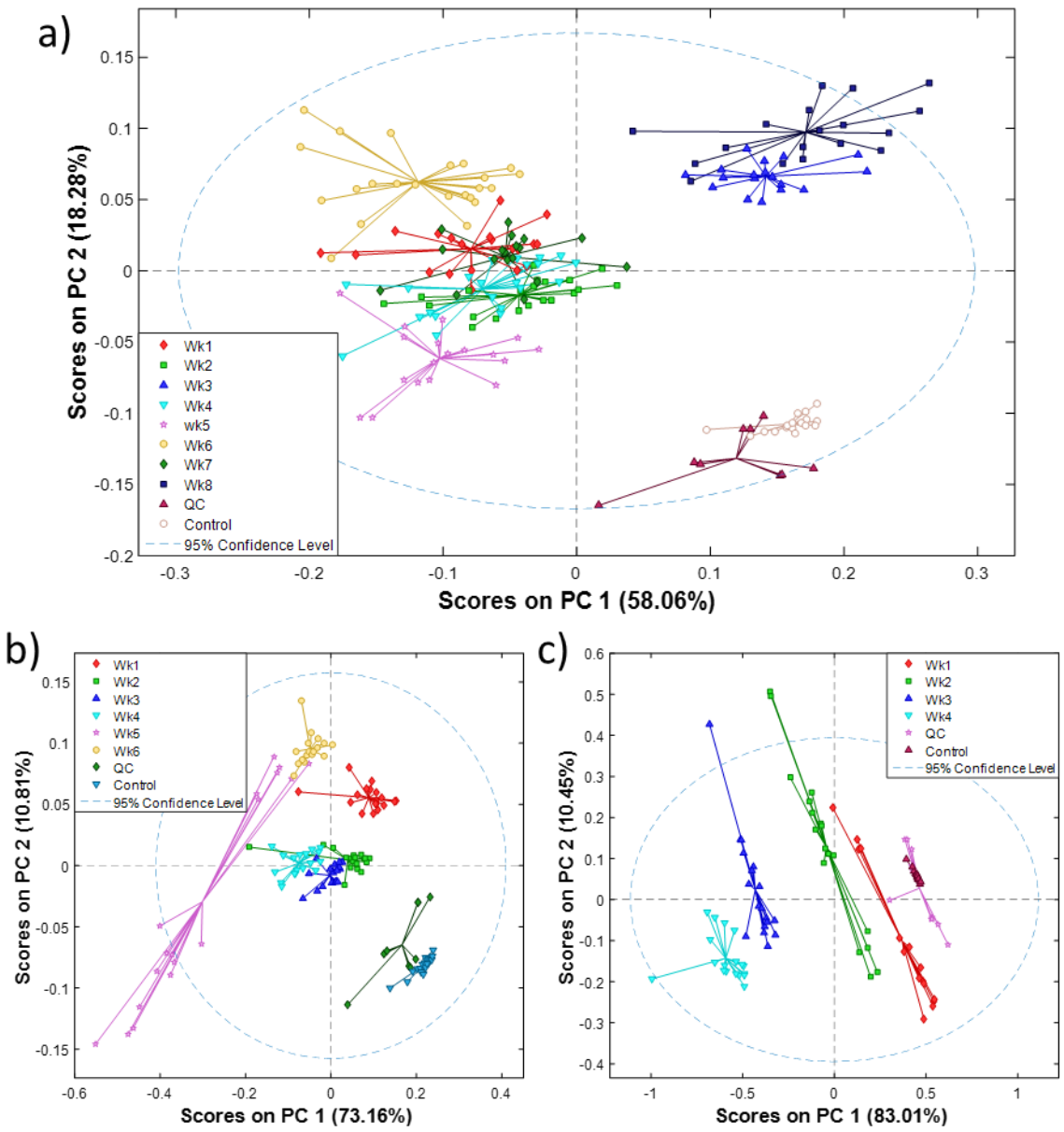

Figure 9. PCA score plots of polyimide films hydrothermally aged a) up to 8 weeks at 70 °C (185 samples × 1738 variables), b) up to 6 weeks at 80 °C (134 samples × 1738 variables), and c) up to 4 weeks at 90 °C (99 samples × 1738 variables).

For all three temperatures, the unaged samples (control and QC) were clustered together and well-separated from the aged samples using two PCs. For the samples that were hydrothermally aged at 70 °C, no distinct clustering or trend was observed within the aged samples. For the dataset of hydrothermal aging at 80 °C, three general clusters explaining 83.97% of the total variance were observed using two PCs: 1) non-aged samples, 2) samples aged for 1 to 4 weeks, and 3) samples aged for 5 to 6 weeks. For the samples that were hydrothermally aged at 90 °C, PC1 alone explained 83.01% of the total variance and different stages of aging were separated mostly by PC1. Of note, the samples aged from 1 to 4 weeks at 80 °C were clustered as one group and could not be easily discerned from one another, whereas the samples aged from 1 to 4 weeks at 90 °C showed a clear week-to-week progression of hydrothermal aging.

The dataset for hydrothermal aging at 90 °C was selected for further analysis, due to the fact that it demonstrated the best separation for the aging process in the PCA score plot. Figure S2 (Supporting Information) shows the baseline and light scatter corrected spectra for the samples aged at this temperature from 1 to 4 weeks. A total of 69 spectra were overlayed and color-coded for different aging durations. The majority of the peaks for the polyimide film were observed at wavenumbers less than 1800 cm^{-1}, while wavenumbers larger than 1800 cm^{-1} in the spectra did not display profound changes from the baseline. To observe the changes of the peaks due to hydrothermal aging in more detail, further analysis was focused on the region from 688 cm^{-1} to 1805 cm^{-1} (580 variables).

With a total of 580 variables from 688 cm^{-1} to 1805 cm^{-1}, another PCA model was constructed with the samples aged at 90 °C only, excluding the control and QC (Figure 10a). With the PC1 model alone, 82.15% of the total variance was explained and the samples that were aged

from 1 to 4 weeks were clustered in a series along the PC1. Figure 10b shows the loading plot of the PCA model constructed from the 69 samples aged at 90 °C for up to 4 weeks.

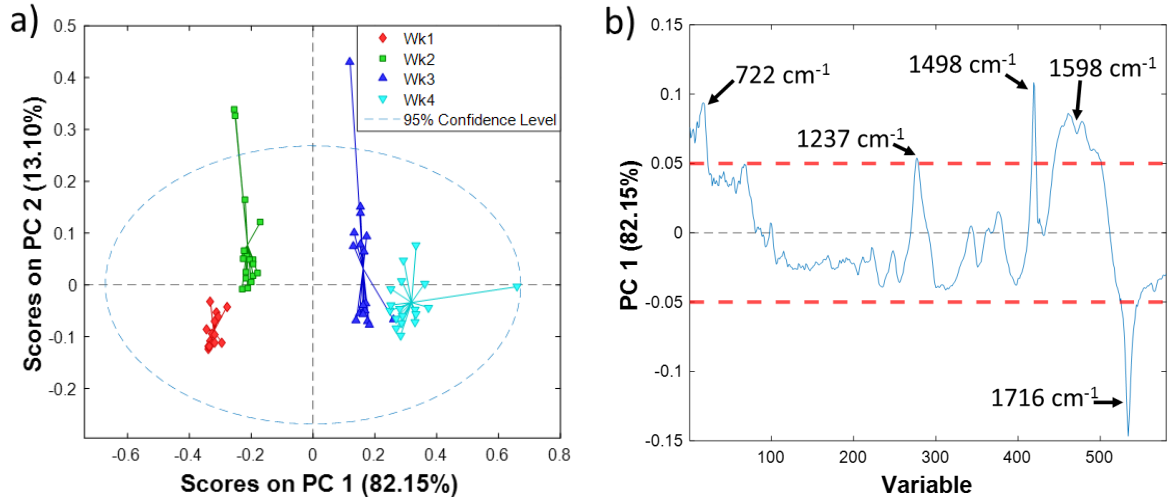

Figure 10. a) PCA score plot of polyimide film hydrothermally aged at 90 °C for 4 weeks (69 samples × 580 variables) b) loading plot of the 580 variables for PC1.

From the loading plot in Figure 10b, the variables with PC1 loadings of less than -0.05 were relevant to samples at an early stage of aging (1–2 weeks). In Figure 11, the variable that is significant for the samples aged 1–2 weeks was labelled with a red asterisk (*), which corresponds to the peak at 1716 cm^{-1} (C=O asymmetric stretching of the imide). This peak decreases over time, which can be attributed to the imide ring being slowly hydrolyzed due to hydrothermal aging. Contrarily, the loadings of PC1 greater than 0.05 were more closely related to samples at later stages of hydrothermal aging (3–4 weeks). The variables selected for the 3–4 week aging period were labelled with a green asterisk (*) in Figure 11, including the peaks at 722 cm^{-1} (C=O bending of imide, out of plane), 1237 cm^{-1} (Ph–O–Ph stretching), 1498 cm^{-1} (C=C stretching), and 1598 cm^{-1} (unassigned).

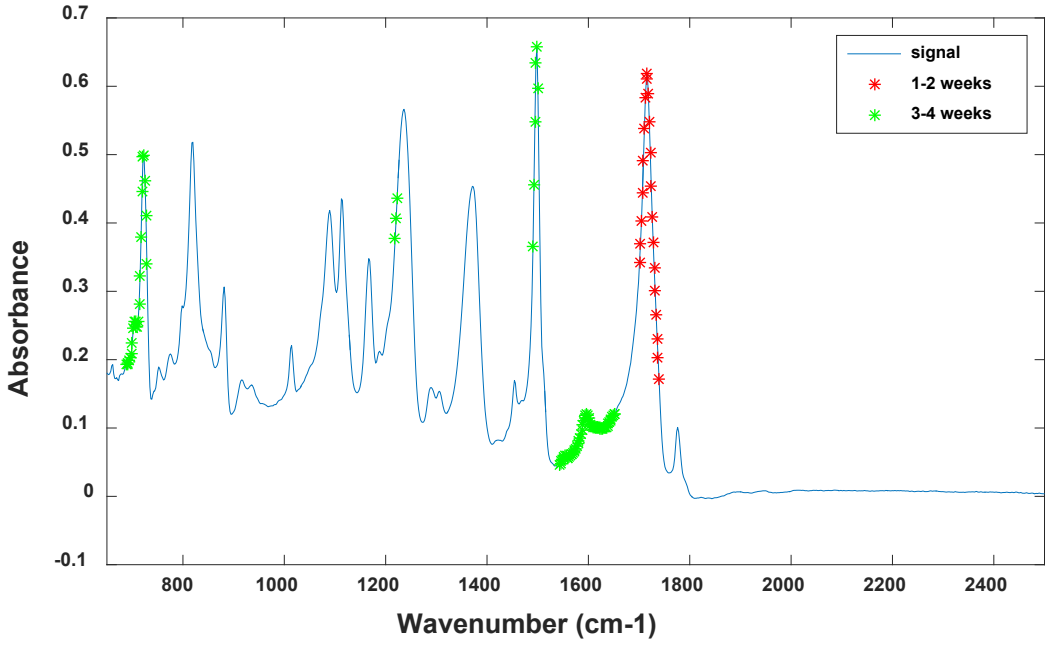

Figure 11. The selected variables for 1-2 weeks and 3-4 weeks from the loading plot of PC1 in Figure 10b.

Based on these results, the preprocessed data (baseline and light scatter corrected data) was used to examine the changes in the peak at 1716 cm^{-1} relative to the peak at 1498 cm^{-1} for all three aging temperatures. While the intensity of the peak 1498 cm^{-1} (the aromatic C=C stretching) did not significantly change, a clear decrease in the peak at 1716 cm^{-1} was observed with aging at all three temperatures, occurring most profoundly with the hydrothermal aging at 90 °C. The ratio between the two peaks (1716 cm^{-1}/1498 cm^{-1}) was calculated and compared to the ratio for the non-aged sample measurements; the ratio decreased 4.0 % after 8 weeks of aging at 70 °C, 8.0 % after 6 weeks of aging at 80 °C, and 25.9 % after 4 weeks of aging at 90 °C. Figure 12 shows the ratio between the two peaks (1716 cm^{-1}/1498 cm^{-1}) at the three temperatures of the hydrothermal aging (Details of the preprocessed peak intensity at 1716 cm^{-1} and 1498 cm^{-1} in Supporting Information, Figure S3).

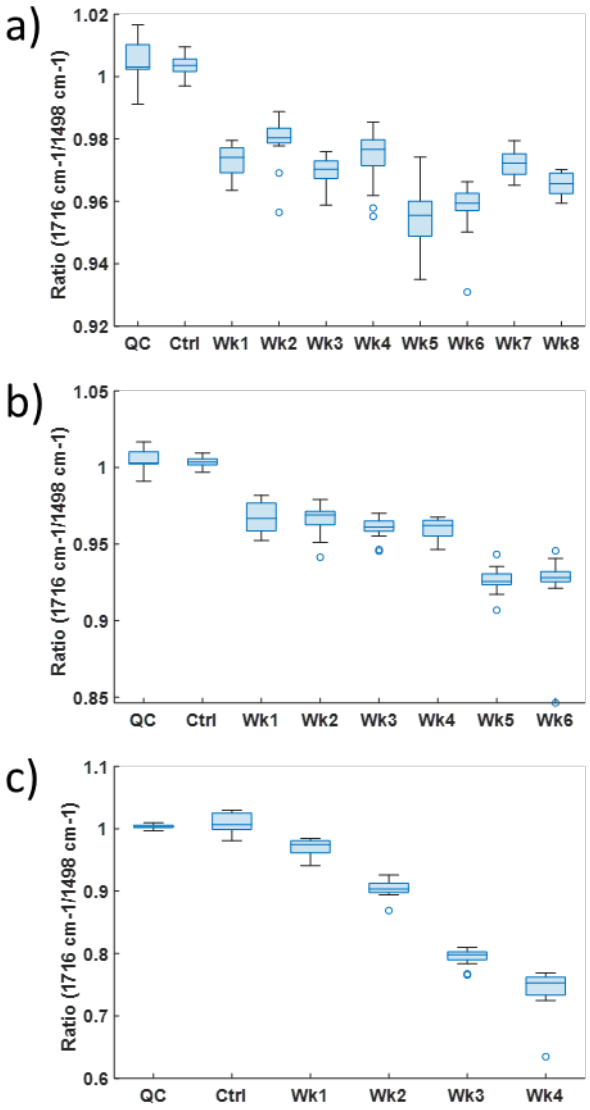

Figure 12. The box plots of the ratio between the two peaks (1716 cm^{-1}/1498 cm^{-1}). a) 70 °C, b) 80 °C, c) 90 °C

The absorbance at 3352 cm^{-1} among the preprocessed spectral datasets was also investigated to evaluate the changes more objectively in the region from 2800–3700 cm^{-1} (O-H and/or N-H stretches) for all three aging temperatures. A general trend of increasing peak intensity was observed for all three aging temperatures (**Figure** S4, Supporting Information). Once again, the most profound changes were observed for the hydrothermal aging at 90 °C, with the absorbance at 3352 cm^{-1} increasing 10-fold from 0.0025 for the non-aged specimens to an average value of 0.0252 for samples that had been aged for four weeks.

4. DISCUSSION

The more profound changes observed in the chemometric analysis of ATR-FTIR data for samples hydrothermally aged at 90 °C are consistent with more profound reductions in mechanical strength of the polyimide films aged at this temperature. Although the ultimate tensile strength decreased to approximately 50 % of the original value for all three temperatures, this degradation took six weeks at 70 °C (83 ± 7 MPa), three weeks at 80 °C (83 ± 4 MPa), and only two weeks at 90 °C (73 ± 5 MPa) (Figure 4). Of note, the UTS value of samples aged at 70 °C seemed to plateau after six weeks and never decreased beyond a 46 % reduction. As a comparison, the results of DeIasi and Russel on the effect of hydrothermal aging in DI water on the tensile strength of polyimide show a plateau in UTS at about 60% of the initial value for aging temperatures of 80 and 100°C.[9a] Furthermore, individual percent elongation at break measurements conducted after a certain aging time showed larger variations for specimens that were aged at 70 °C (particularly between 48–120 hours in Figure 5). Chemometric analysis of ATR-FTIR data also produced a unique PCA score plots for the hydrothermal aging at 70 °C relative to the higher temperatures of 80 and 90 °C. Despite the longer duration, only two clusters were observed in the PCA score plot (Figure 9) corresponding to unaged and aged samples. In contrast, the hydrothermal aging at 80 °C formed three clusters corresponding to unaged, an early stage of aging, and a later stage of aging while at 90 °C a more distinct week-to-week aging progression was observed. The results discussed above all suggest that the hydrothermal aging is less controlled and more sporadic at the lower temperature of 70 °C. However, these results also clearly demonstrate that even at temperatures below 100 °C, the mechanical integrity of polyimide is affected by hydrothermal aging.

As alluded to in the introduction, there exists some uncertainty in the literature regarding which chemical groups are causing the loss of mechanical integrity that occurs upon hydrothermal aging, as imide groups are difficult to hydrolyze under neutral conditions.[9] In order to obtain more insight, the differences between the ratio of the peak intensities of the imide C=O stretching at 1716 cm^{-1} and the aromatic stretching (C=C) at 1498 cm^{-1} (Figure 12) were compared. Whereas a reduction in the peak at 1716 cm^{-1} was observed upon hydrothermal aging at all three temperatures, the peak at 1498 cm^{-1} did not change significantly. This is consistent with an increase in intensity at 3352 cm^{-1} which was also observed upon aging at all three temperatures, corresponding to an increase in O-H and/or N-H functional groups. These results signify that the imide ring is indeed being hydrolyzed and converted to carboxylic acid and/or amide groups, even at temperatures as low as 70 °C. This contradicts the proposition made by DeIasi and Russel that the reduced strength resulting from the hydrothermal aging of polyimide below 100°C is due to the hydrolysis of amide or carboxylic acid groups rather than imide rings.[9a]

As prefaced in the introduction, there is an interest in finding high performance, heat-resistant polymers that mimic the hydrothermal degradation of fire protective clothing. Such materials are desired in order to construct sensors that are able to signal the end-of-life for fire protective clothing. A hydrothermal aging study performed on fire protective fabrics by monitoring the breaking force retention after prolonged immersion in water at temperatures between 60 and 90°C found an activation energy for the hydrothermal degradation that ranged from approximately 53 to 65 kJ/mol for Kevlar®/PBI fabric blends.[20] These values are quite comparable with that of the polyimide film in this study (E_a = 71.8 kJ/mol), suggesting that this polymer is a viable candidate for the construction of a hydrothermal sensor for fire protective fabrics.

5. CONCLUSIONS

Despite a strong reputation for thermal and chemical stability of polyimides, a decrease in ultimate tensile strength and percent elongation at break, as well as the chemometric analysis of ATR-FTIR data all clearly indicate the moisture-based degradation of the commercial polyimide used in this study. Furthermore, chemometric analysis of the ATR-FTIR spectra of aged samples strongly suggests that significant hydrolysis of the imide groups does indeed occur, even at temperatures as low as 70 °C, and this likely contributes to the loss of mechanical properties that occurs upon prolonged hydrothermal aging.

In addition to the above, the activation energy for the hydrothermal degradation of the polyimide film was calculated to be 71.8 ± 0.1 kJ/mol from an Arrhenius plot using the UTS data of aged samples. This value is comparable with the activation energy for the moisture-based degradation of actual fire protective clothing (53–65 kJ/mol) which was calculated under similar conditions and therefore suggests the promising potential of commercial polyimide to be used to mimic the hydrothermal aging of fire protective clothing. Future work will include further investigation on the use of commercial polyimide film as a sensing component in an end-of-life sensor for fire protective clothing. Another important result of this research is the evidence of the large potential of chemometrics for polymer aging studies as it allows identifying degradation mechanisms from subtle chemical changes in the materials.

Acknowledgements

This project has received a funding from the Natural Sciences and Engineering Research Council of Canada (NSERC) (STPGP 521866 - 18). The authors also want to acknowledge the support provided by the Analytical and Instrumentation Laboratory and Mr. Wayne

Moffat in the Chemistry Department, and thank Dr. Anastasia Elias for the use of her mechanical test frame and Mr. H. Pisavadia for the help with the figure revision.

Received: ((will be filled in by the editorial staff))
Revised: ((will be filled in by the editorial staff))
Published online: ((will be filled in by the editorial staff))

References

[1] a) R. G. Bryant, in *Ullman's Encyclopedia of Industrial Chemistry*, Wiley-VCH, Weinheim, Germany, **2014**, Polyimides. L.; b) L. W. McKeen in *Film Properties of Plastics and Elastomers, 4th edition* (Ed: L. W. McKeen), Science Direct, **2017**, Ch. 7; c) C. E. Sroog, *Prog. Polym. Sci.*, **1991**, *16*, 561.

[2] a) D.-J. Liaw, K.-L. Wang, Y.-C. Huang, K.-R. Lee, J.-Y. Lai, C.-S. Ha, *Prog. Polym. Sci*., **2012**, *37*, 907; b) I. Gouzman, E. Grossman, R. Verker, N. Atar, A. Bolker, and N. Eliaz, *Adv. Mater*., **2019**, *31*, 1807738.

[3] V. E. Ogbonna, A. P. I. Popoola, O. M. Popoola, S. O. Adeosun, *Polym. Bull.*, **2020** (early access)

[4] Z. Xu, Z. L. Croft, D. Guo, K. Cao, G. Liu, *J. Polym. Sci.*, **2021** (early access)

[5] a) H.-J. Ni, J.-G. Liu, Z.-H. Wang, S.-Y. Yang, *J. Ind. Eng. Chem.*, **2015**, *28*, 16; b) P. K. Tapaswi, C.-S. Ha, *Macromol. Chem. Phys*., **2019**, *220*, 1800313; c) X. Wu, C. Shu, X. He, S. Wang, X. Fan, Z. Yu, D. Yan, and W. Huang, *Macromol. Chem. Phys*., **2020**, *221*, 1900506.

[6] a) W. S. Li, Z. X. Shen, J. Z. Zheng, S. H. Tang, *Appl. Spectrosc*., **1998**, *52*, 985; b) K. Iida, Y. Imamura, C. Liao, S. Nakamura, G. Sawa, *Polym. J.*, **1996**, *28*, 352; c) R. W. Snyder, *Macromolecules*, **1989**, *22*, 4166.

[7] a) S. Z. Li, R. S. Chen, S. G. Greenbaum, *J. Polym. Sci., Part B: Polym. Phys*., **1995**, *33*, 403; b) H. N. Sharma, M. P. Kroonblawd, Y. Sun, E. A. Glascoe, *Sci. Rep.*, **2018**, *8*, 16889; c) J. Seo, A. Le, J. Oh, and H. Han, *Polym. J.*, **2000**, *32*, 583; d) J. Seo, H. Han, *J. Polym. Sci.*, **2001**, *82*, 731; e) S. Niyogi, S. Maiti, B. Adhikari, *Polym. Degrad. Stab.*, **2000**, *68*, 459; f) R.

Subramanian, M. T. Potriger, J. H. Morris, J. P. Curilla, *Mat. Res. Soc. Symp. Proc.*, **1991**, *227*, 147; g) D. K. Yang, W. J. Koros, H. B. Hopfenberg, V. T. Stannett, *J. Appl. Polym. Sci*., **1985**, *30*, 1035.

[8] a) S. G. L. Chen, T. Hsien (Industrial Technology Research Institute), *Japan 4,761,710*, **1988**; b) J. Boudaden, M. Steinmaßl, H.-E. Endres, A. Drost, I. Eisele, C. Kutter, P. Müller-Buschbaum, *Sensors*, **2018**, *18*, 1516; c) A. R. K. Ralston, C. F. Klein, P. E. Thoma, D. D. Denton in *Proceedings of the International Solid-State Sensors and Actuators Conference - TRANSDUCERS '95*, IEEE, Stockholm, Sweden **1995**, 821; d) A. R. K. Ralston, M. C. Buncick, D. D. Denton, *TRANSDUCERS '91: 1991 International Conference on Solid-State Sensors and Actuators. Digest of Technical Papers*, IEEE, San Francisco, U.S.A. **1991**, 759.

[9] a) R. Deiasi and J. Russell, *J. Appl. Polym. Sci*., **1971**, *15*, 2965. b) Y. Xu, A. T. Zehnder, *Extreme Mech. Lett*., **2017**, *16*, 49; c) Y. Xu, A. T. Zehnder, *Exp. Mech.*, **2017**, *57*, 857.

[10] W. Lincoln-Hawkins, *Polymer Degradation and Stabilization*, Springer, Berlin, Heidelberg, **1984**.

[11] a) K. Kumar, *Resonance*, **2017**, *22*, 747; b) R. Bro, A. K. Smilde, *Anal. Methods*, **2014**, *6*, 2812.

[12] a) Y. Y. Wang, J. Q. Li, H. G. Liu, Y. Z. Wang, *Molecules*, **2019**, *24*, 2210; b) D. Custers, T. Cauwenbergh, J. L. Bothy, P. Courselle, J. O. De Beer, S. Apers, E. Deconinck, *J. Pharm. Biomed. Anal*., **2015**, *112*, 181; c) F. N., Arslan, F. Caglar, *Food Anal. Methods*. **2019**, *12*, 355.

[13] a) A. R. Horrocks, *Polym. Degrad. Stab.*, **2011**, *96*, 377; b) P. I. Dolez, T. Vu-Khanh, *Int. J. Occup. Saf. Ergon.*, **2009**, *15*, 347.

[14] M. McQuerry, S. Klausing, D. Cotterill, E. Easter, *Fire Technol.*, **2015**, *51*, 1149.

[15] P. Dolez, H.-J. Chung, C. Cho, End-of-Life Sensors for Fabrics. United States. U.S. Provisional Patent Application 63/156,143. 2021/03/03

[16] a) C. Arrieta, E. David, P. Dolez, T. V.-Khanh, *J. Appl. Polym. Sci.*, **2010**, *15*, 3031; b) J. Verdu, Techniques De L'ingénieur: Traité Plastiques et Composites. Vol. *AM3152*; Paris, France: Techniques de l'Ingénieur, **2002**; c) P. I. Dolez, N. S. Tomer, Y. Malajati, J. Appl. Polym. Sci., 2019, 136, 47045.

[17] K. T. Gillen, M. Celina, R. L. Clough, J. Wise, *Trends Polym. Sci*., **1997**, *5*, 250.

[18] L. C. Lee, C. Y. Liong, A. A. Jemain, *Chemom. Intell. Lab. Syst.,* **2017**, *163*, 64.

[19] B. Wise, N. Gallagher, R. Bro, J. Shaver, W. Windig, R. Koch, *Chemometrics Tutorial for PLS_Toolbox and Solo*, **2006**, Eigenvector Research, Inc., Wenatchee, WA.

[20] Md. S. Hoque, A. Saha, H.-J. Chung, and P. I. Dolez, presented at 32nd Canadian Materials Science Conference, virtual, June **2021**.